Research Article Vol. 15, No. 1 / 1 Jan 2024 / Biomedical Optics Express 199
Biomedical Optics EXPRESS

Organelle-specific phase contrast microscopy (OS-PCM) enables facile correlation study of organelles and proteins

CHEN CHEN,[1] ZACHARY J. SMITH,[1,2] JINGDE FANG,[1,4] AND KAIQIN CHU[2,3,5]

[1]*Department of Precision Machinery and Precision Instrumentation, University of Science and Technology of China, Hefei, Anhui 230027, China*
[2]*Key Laboratory of Precision Scientific Instrumentation of Anhui Higher Education Institutes, University of Science and Technology of China, Hefei, Anhui 230027, China*
[3]*Suzhou Institute for Advanced Research, University of Science and Technology of China, Suzhou, Jiangsu 215123, China*
[4]*jdfang@mail.ustc.edu.cn*
[5]*kqchu@ustc.edu.cn*

Abstract: Current methods for studying organelle and protein interactions and correlations depend on multiplex fluorescent labeling, which is experimentally complex and harmful to cells. Here we propose to solve this challenge via OS-PCM, where organelles are imaged and segmented without labels, and combined with standard fluorescence microscopy of protein distributions. In this work, we develop new neural networks to obtain unlabeled organelle, nucleus and membrane predictions from a single 2D image. Automated analysis is also implemented to obtain quantitative information regarding the spatial distribution and co-localization of both protein and organelle, as well as their relationship to the landmark structures of nucleus and membrane. Using mitochondria and DRP1 protein as a proof-of-concept, we conducted a correlation study where only DRP1 is labeled, with results consistent with prior reports utilizing multiplex labeling. Thus our work demonstrates that OS-PCM simplifies the correlation study of organelles and proteins.

1. Introduction

Organelles are important functional subunits of cells where they regulate the cell state and accomplish various physiological activities [1]. For example, mitochondria provide energy and modulate stress response for cellular activities and health, or the endoplasmic reticulum (ER), which is involved in the synthesis and processing of intracellular proteins [2]. Organelles also interact with each other to regulate a variety of physiological activities through membrane contact and fusion, which facilitates the production and transportation of proteins, lipids and other substances in the cell. This means that many proteins are closely associated with organelles. Through the correlative study of the temporal and spatial distribution of both the organelles and proteins, insights about the functions of those structures and physiological state of the cell can be revealed. On the other hand, the misdistribution of organelles and proteins is usually associated with cellular dysfunction and disease such as cancer and Alzheimer [3].

Currently, the study on the spatial distribution of organelles and proteins is mainly accomplished through fluorescence imaging [4,5]. However, the phototoxicity associated with fluorescent labeling causes cell damage and the photobleaching prevents long term observation of cell activities [6]. In addition, the cell membrane and nucleus are the natural inner and outer boundaries for many organelles and proteins in a cell. Accordingly, they are often used as two important landmark structures to analyze the spatial distribution of organelles and proteins [7,8].

#510243 https://doi.org/10.1364/BOE.510243
Journal © 2024 Received 25 Oct 2023; revised 29 Nov 2023; accepted 3 Dec 2023; published 14 Dec 2023

Biomedical Optics EXPRESS

To this end, it is often necessary to label the nucleus and cell membrane in addition to the proteins and organelles of interest. Yet, this multiple labeling greatly increases the complexity of sample preparation and requires multiple fluorescence channels. More importantly, the adverse effect from label-induced phototoxicity and photobleaching are greatly increased due to the large surface and volume of the landmark structures [6].

Label-free imaging methods such as quantitative phase microscopy offer attractive alternatives due to their ability to image samples for a long time with minimal photo-damage [9,10]. The image contrast in phase microscopy is derived from intrinsic signals, i.e., the refractive index distribution of the sample. However, phase microscopy techniques lack specificity and it is difficult to segment and determine the types of subcellular structures without *a priori* knowledge. Recently deep learning techniques have made tremendous progress in cell recognition [11,12]. However, segmentation success at the subcellular level is still scarce in the literature due to the low resolution of most label free images [13,14]. Note that in order to perform correlation study between organelle and protein, the morphology of the organelle should be well resolved in the image. When the resolution and contrast of the label-free image lacks subcellular detail, deep-learning can, at best, make educated guesses about organelle distribution. Among the few successes reported to date [15–18] our technique (termed organelle-specific phase contrast microscopy, OS-PCM) has been shown to accurately recognize various organelles in an unlabeled cell due to the high resolution and contrast in images acquired by our phase microscope [19]. We have reported the first success of obtaining detailed morphology of mitochondria as well as the studying of organelle interactions using unlabeled cell images [16,20]. To briefly recap OS-PCM, high resolution, high contrast phase images are acquired using our ultra-oblique phase contrast microscopy instrument. The phase channel performs panoramic imaging of the cell where organelles of interest and the important boundaries of the cell are automatically identified via a neural network. Our phase contrast microscope can be naturally coupled with fluorescence. Therefore, previously we have used a fluorescent channel to generate ground-truth data of organelle distributions for training artificial intelligence networks for organelle segmentation. In doing so we have accurately segmented mitochondrial networks, lysosomes, and lipid droplets which have been used to study mitochondrion-lysosome interaction under different physiological conditions [20], as well as coupled to Raman spectroscopy for facile *in situ* lipid droplet profiling [21].

To date, however, we have focused on larger organelle-level structures which can be well imaged by our label-free microscope, and the fluorescence channel is used simply to provide ground truth information for training a deep network. Here, we will further explore the application of this technology in the correlation study of proteins and organelles, where the fluorescence channel is used to image protein distributions that are still beyond the reach of label-free methods. However, in contrast with pure fluorescence-based methods [4,5,22], where at least 3 or 4 labels are required for organelles and protein of interest as well the nucleus and cell membrane, here we only need to label the protein, while information such as the target organelle and cellular landmark information can be obtained through OS-PCM. By eliminating the need to stain organelles and landmark structures, whose sizes are several orders of magnitude larger than that of proteins, our method has the promise to greatly reduce the volume or amount of labelling and the associated phototoxicity, thus facilitating the study of cellular activities and dynamics with minimal interference. For example, mitochondria respond to oxidative stress, and thus the ability to obtain their spatial distribution without phototoxicity is beneficial to the study of their function with minimum experimental interference [23]. Here we use OS-PCM to perform panoramic imaging of the cell where organelles of interest and the important boundaries of the cell are automatically identified. Simultaneously, a fluorescence channel images the labeled protein. In this way, we obtain the distribution of organelles and proteins and their relative positions in a cell, which are further used to analyze their interactions under different physiological conditions.

Biomedical Optics EXPRESS

In this work, mitochondria and the protein DRP1 are used as an example to demonstrate the capability of OS-PCM in the correlation study of organelle and protein. Mitochondria, as discussed above, are under extensive study by biologists due to its important roles in cell state and disease [24]. DRP1 is found previously to be not only associated with the fission of the mitochondria [25] but also involved in other cellular activities [4]. Previous study on their correlation are based on multiple fluorescence labeling [5,26]. Here we wish to conduct a similar study with a single labeling. We will first use OS-PCM to collect cell images where mitochondria, nuclei and cell membranes are unlabeled, and train deep learning networks to identify them automatically. Further we will also develop automatic analysis to obtain the spatial distribution of mitochondria and DRP1 with respect to the cell's inner and outer boundaries. Typical correlation studies of DRP1 and other organelles rely on multiple labeling and analyze only a few small regions of interest selected from a cell image [4,5,27]. With OS-PCM, we can examine the whole cell with high spatial and temporal resolution, easily obtaining time lapse data. In this work, we found that the ratio of DRP1 colocalized with mitochondria is about 30% in a normal cell, which is consistent with prior report [26]. An important aspect of the OS-PCM method is that, while automatic organelle recognition can be accomplished by a trained network, the underlying, panoramic phase image is always available. Thus, for example, when we observed DRP1 aggregates that were not co-localized with mitochondria, we could return to the label free phase image and determine where in the cell the DRP1 aggregates were (in this case, primarily on the ER). In a traditional fluorescence experiment, by contrast, anything that is not expressly labeled is completely "invisible" to the experimenter. We further emphasize that in this study we obtained this plethora of quantitative information using a system where only the DRP1 protein needs be labeled. Thus, we have demonstrated that OS-PCM plus a single fluorescent channel is an attractive alternative to multiplex fluorescence imaging for the study of organelle and protein interactions.

2. Materials and methods

2.1. High resolution multimodal microscopy

Our OS-PCM system has both phase and fluorescence channels, as shown in Fig. 1. For a detailed description of the instrument, please refer to our prior report [16]. Briefly, a circular LED with a center wavelength of 505 nm was used as the light source for the phase channel. Both scattered and non-scattered light were collected through a Nikon Plan Apo 60X objective lens with a numerical aperture (NA) of 1.49. The non-scattered light was modulated by a spatial light modulator (Meadowlark Optics, ODPDM512-0532-P8) with a phase shift of $\pi/2$ and an attenuation of OD1 using a ring-shaped mask. The fluorescence channel utilized a 577 nm laser (Changchun Xinchuang Optoelectronic Technology, MGL-F-577) as the light source, and is separated from the phase channel through a dichroic mirror (Thorlabs, FELH0600). Both channels had similar spatial resolution of ~250 nm, identical magnification (120x) and fields of view (~200um), The images were captured using sCMOS cameras (Andor, ZYLA-4.2P-CL10), and data acquisition was controlled by LabVIEW. In this work, we have used a relatively thin cell (COS 7) to study the correlation between mitochondria and DRP1. As such, we have collected 2D images and the subsequent analysis and conclusions are thus limited to thin cells.

The registration of the phase and fluorescence channels was achieved by obtaining a registration matrix from captured images of microspheres (co-registered beads images are shown in Supplement 1 Fig. S1). This matrix was then used to perform transformation on the protein images.

Biomedical Optics EXPRESS

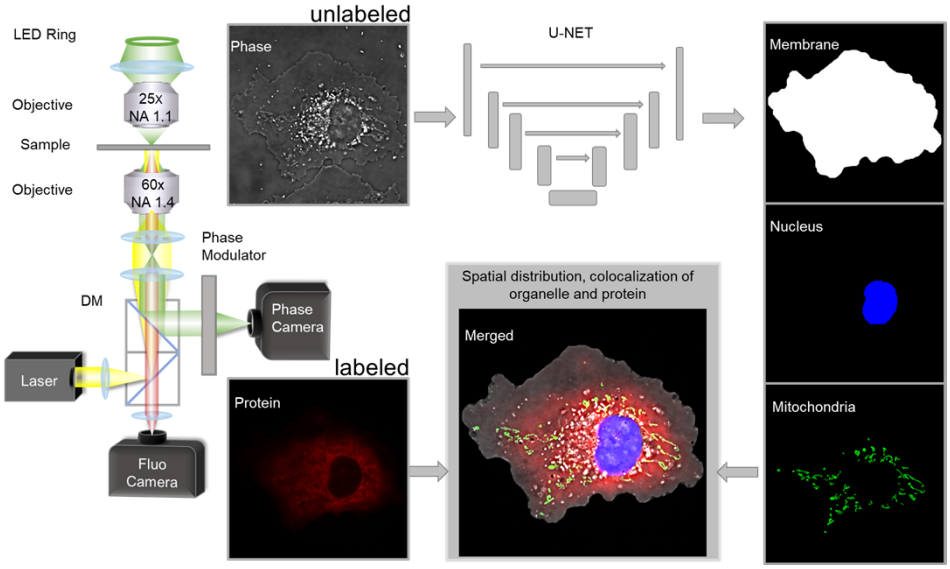

Fig. 1. Overview of the correlation study between organelles and proteins using OS-PCM. Two-dimensional cell image is collected through the phase channel where the organelles (mitochondria is used as an example here), nucleus and cell membrane are identified through trained CNN networks. Protein images are obtained through the fluorescent channel. Automatic morphology analysis are performed to obtain the positional information for the correlation study of proteins and organelles.

2.2. Automatic segmentation of specific structures through neural networks and their training

As both mitochondria and DRP1 are highly dynamic, in this proof of concept study, we will perform correlation studies based on 2D images. The phase images are acquired with phase shifting fixed at $\pi/2$, which is different than what we have used in our previous works [16,20]. In our previous mitochondria prediction works, we have either used 3D SLIM images with similar resolution or 2D images with a higher resolution (a different system with blue LED illumination). These changes both simplify and speed up the image acquisition process (as 3D images and phase shifting were not performed). However, this places a higher burden on the deep learning network to identify the mitochondria and other structures. Thus in terms of mitochondria prediction for the purpose of this work, we collected new training and testing data and retrained our previously-reported mode. A total of 460 pairs of fluorescence and phase images of COS7 cells (among which 100 are new) are used for the training and testing of mitochondria prediction neural network. For nuclei and cell membrane recognition, brand new models are constructed and trained with a 300 pairs of nucleus images and 99 pairs of cell membrane images. All data were divided into training and testing sets in an 80:20 ratio. Mean Square Error (MSE) was employed as the loss function for all training processes. Structural similarity index measure (SSIM) is used for the evaluation of the prediction accuracy of mitochondria and Pixel Accuracy (PA) for nucleus and membrane respectively.

While our previous work [16] has shown that the networks can be generalized to other cell types, the neural network would likely need to be retrained using example data of other cell types for optimum performance. Additionally, the cells studied here are thin, such that membrane, nucleus, and mitochondria can be well resolved using a single 2D image. For thicker cells where

Biomedical Optics EXPRESS

these objects are not co-planar, 3D imaging may be required, which would come at a cost to temporal resolution.

2.3. Image preprocessing and distance analysis

In order to obtain DRP1 aggregate images, we have followed a procedure outlined in Ref. [5]. First we used the imageJ plugin 'Rollingball' to remove the diffusive background in the fluorescence image. The ball radius was selected as 5 pixels based on the average outer diameter of the DRP1 oligomer (~120 nm [28]) and the system resolution (54.2 nm per pixel). Then a value of 99.9% of the maximum intensity is used as the threshold to obtain the binarized image. After morphological operations such as removing small targets and dilation, DRP1 aggregate images are obtained. The number of aggregate is reported to increase during cell apoptosis [5].

The spatial distribution of organelles or proteins can be determined by their positions in the segmented images. Information about their positions (distances) Localizing them with respect to the inner and outer boundaries of the cell is advantageous for analyzing their functions [8,22]. Following prior work based on multiple labeling, here we can obtain the distance information with a single labeling. To achieve this, we binarized the recognized nucleus and cell membrane in the phase image and obtained the edges of these landmark objects. Mitochondria and DRP1 were then measured with respect to these edges. For mitochondria, the recognized mitochondria from the phase images are further binarized by 'Mitometer' which is a recently developed mitochondria analysis tool [29]. With the boundary information of mitochondria, cell membrane, and nucleus, we can calculate their distances with respect to each other. Using the line formed by the centroids of mitochondria and nucleus, we can locate the corresponding boundaries of the nucleus and cell membrane and the consequent distances from mitochondria to the nucleus $D_{mito-nuc}$ and from mitochondria to the cell membrane . This allows us to calculate the distances of mitochondria to the nucleus relative to $D_{mito-mem}$ the cell width along the same axis:

$$D^{rel}_{mito-nuc} = \frac{D_{mito-nuc}}{D_{nuc-mem}}$$

where $D_{nuc-mem} = D_{mito-nuc} + D_{mito-mem}$, and represents the cell width along the vector connecting the mitochondria and nucleus centroids. Naturally, then, the relative distance between the mitochondria and the membrane is 1-$D^{rel}_{mito-nuc}$. Arbitrarily selecting the horizontal direction as 0 degrees, the distances of individual mitochondria can then be parsed and grouped together based on their angular position within the cell.

Similarly, we can compute the relative distance for the protein as well and here we use $D^{rel}_{\mathrm{DRP1}-nuc}$ to represent the relative distance of DRP1 to the nucleus. For the cell-level analysis, the mean value of the relative distances is used and consequently we have $\bar{D}^{rel}_{mito-nuc}$ and $\bar{D}^{rel}_{DRP1-nuc}$ to represent the mean relative distance of mitochondria and DRP1 respectively.

2.4. Sample preparation

In this paper, following prior reports [8,30], COS 7 cells were cultured to study the correlation of mitochondria and DRP1 with a single label. Standard preparation procedures are used to culture, transfect and treat cells, and complete details can be found in the Supplement 1.

3. Results

3.1. OS-PCM methodology of correlation study between organelles and proteins

Figure 1 provides an overview of the OS-PCM method. Unlabeled organelles, as well as the cell nucleus and cell membrane, are captured using high-resolution phase contrast microscopy and identified using a trained CNN. Protein images are obtained through the fluorescent channel of the microscope. Here, we use mitochondria and the associated protein DRP1 as an example to

Biomedical Optics EXPRESS

demonstrate the performance of OS-PCM. The prediction accuracy for the mitochondria is 0.9289 (SSIM), 98.73% and 96.14% (PA) for nuclei and membrane respectively. More quantitative results of mitochondrial, nucleus, and cell membrane recognition can be found in the Supplement 1 Figures S2 and S3. With the prediction results, one can obtain morphological information of the cell membrane, cell nucleus, mitochondria automatically through the analysis methods described in 2.3. Number and spatial distribution of DRP1 aggregates can also be obtained using methods described in 2.3. Thus we can easily examine their colocalization and changes due to treatment, their movements to each other and with respect to the inner and outer boundaries of the cell. Since only protein labeling is performed and the volume of protein is orders of magnitude smaller than organelles, nucleus and membrane, the OS-PCM method greatly reduces the impact of photobleaching compared to traditional methods which require multiple labeling, allowing for long term observation of cellular activities.

3.2. Automatic analysis of the spatial distribution of mitochondria and DRP1 in cells

As mentioned in the introduction, to study the spatial distribution of DRP1 and mitochondria, it is essential to not only obtain the positional information of these two objects but also relate them to important cellular landmarks, typically the cell nucleus and membrane. As described in Section 3.1, mitochondria, the cell nucleus, and the cell membrane can be identified from phase channel of OS-PCM without fluorescent labeling. Figure 2(a) shows an example of the phase image of cell membrane, nucleus, and mitochondria, along with their 2D prediction results. By combining these identification results (Fig. 2(b)), we can clearly observe the distribution of mitochondria within the cell, particularly their proximity to the inner and outer boundaries. To quantify the distribution of mitochondria, we calculate the distances of mitochondria with respect to the cell nucleus and cell membrane, as shown in Fig. 2(c). Details about the distance calculation can be found in Methods and materials. We find that the distances of mitochondria to the cell nucleus $D_{mito-nuc}$ and the distance to the cell membrane $D_{mito-mem}$ exhibit a consistent trend. Specifically, mitochondria tend to be closer to the cell nucleus in regions where the cell membrane contracts, while they tend to move away from the nucleus and approach the cell membrane in regions where the cell membrane expands. Thus, the mitochondria tend to prefer a relatively meridional position distribution in COS7 cells. We will further explore and analyze the spatial distribution of mitochondria in the subsequent section.

DRP1 can exist both as monomers and as aggregates inside a cell and show up as both diffuse and punctate distributions in fluorescence images (as shown in the top image of Fig. 2(d)). The punctate distribution represents the formation of molecular aggregates (rings in this case), which are commonly associated with mitochondrial fission [25]. After obtaining the fluorescence images of DRP1 using OS-PCM, we applied the Rolling Ball background subtraction in ImageJ and then utilized a thresholding method to extract DRP1 aggregates (detailed steps can be found in the Materials and Methods section), with results shown in the bottom image of Fig. 2(d). By merging the segmentation results of DRP1 with those of the mitochondria, the cell nucleus and the membrane, we obtained the combined image as shown in Fig. 2(b). One can see that DRP1 aggregates are distributed both in the cytoplasm region and on mitochondria (as exemplified in Fig. 2(e)). Based on the cumulative distribution of the distances between DRP1 and mitochondria (as shown in Fig. 2(f)), we found that some DRP1 aggregates do not co-localize with mitochondria but remain relatively close to them. The colocalization of DRP1 and mitochondria suggests the involvement of DRP1 in the mitochondria dynamics (more specifically fission). In the depicted cell shown in Fig. 2, approximately 30% of DRP1 aggregates were found on mitochondria, a number which is consistent with previous reports based purely on fluorescence imaging and through manual analysis [26]. Note that here colocalization is defined as the distance between DRP1 and mitochondria being less than 300 nm. Nevertheless, it is clear that not all DRP1 aggregates are on mitochondria.

Biomedical Optics EXPRESS

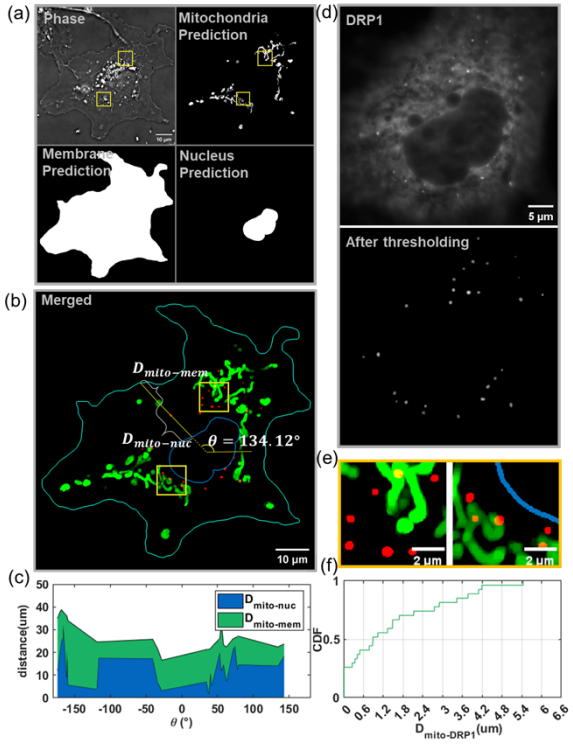

Fig. 2. Images by OS-PCM and the extracted information. (a) Identification of mitochondria, cell membrane and nucleus from the phase image. (b) Merged images based on the identification results(green: mitochondria; Red: DRP1 aggregate; Blue: nucleus; cyan: cell membrane) where the direction and the distance of the mitochondria with respect to the nucleus and membrane are marked as θ, $D_{mito-nuc}$ and $D_{mito-nuc}$ respectively;(c) The distribution of the distances between mitochondria and the cell nucleus or cell membrane showing that they are highly correlated;(d) Segmentation results of DRP1 aggregate using thresholding.(e) Two examples of DRP1 on or near mitochondria;(f) CDF(Cumulative Distribution Function) of the distance between DRP1 and mitochondria. Scale bars in (a,b,d) represent 10 μm and in (e) 2 μm.

In order to find out where non-mitochondrial DRP1 aggregates are, we can exploit one of the key advantages of the OS-PCM method, described in the introduction, where we can return to the original, panoramic phase images. Due to our phase microscope's exquisite contrast and resolution, these images provide information about essentially all of the membrane-bound structures within the cell, including even fine and dim structures such as the ER. As shown in Fig. 3 (Left), by examining the phase images carefully, we can observe that most of the non-mitochondrial DRP1 aggregates are actually found on the endoplasmic reticulum, which can be seen by our phase microscope [19]. In addition, examples of dynamic behavior between DRP1 aggregates and mitochondria can be seen in Fig. 3 (Right).

3.3. *Consistency of the relative distribution of mitochondria within cells*

In the previous section, it was shown that mitochondria exhibit consistency in their relative positions to the cell nucleus and membrane. To determine if this phenomenon is universal, we analyzed 10 cells of different sizes and shapes. The results are shown in Fig. 4.

Biomedical Optics EXPRESS

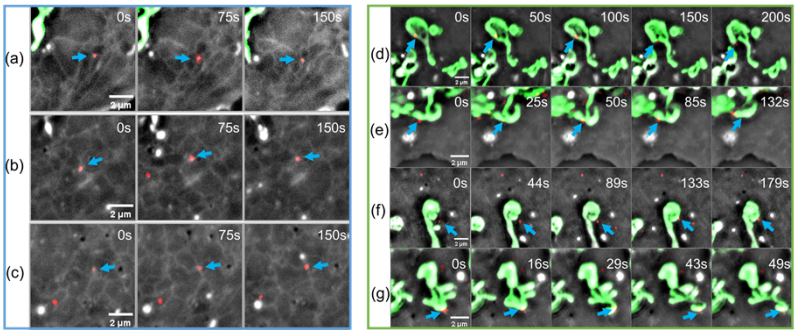

Fig. 3. Left: Examples of DRP1 colocalization with the endoplasmic reticulum during the observed time period. Blue arrows point to DRP1 aggregates and the net-like structures are ER. The green-colored structures in (a) are mitochondria. Right: 4 Various dynamic behavior of DRP1 and mitochondria. (d) DRP1 is directly involved in mitochondrial fission. (e) DRP1 is observed to move on the mitochondria but does not induce fission. (f) DRP1 originally in the cytoplasm moves toward mitochondria, establishing stable contact with mitochondria for a certain period of time. However, during this contact, there is no mitochondrial fission. (g) DRP1 remains on mitochondria during mitochondrial movement. Scale bars in (a-g) represent 2 μm.

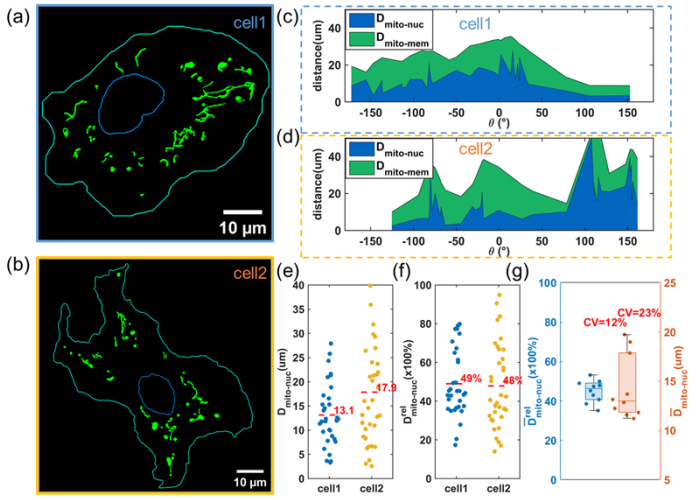

Fig. 4. Distribution of mitochondria in cells of different shapes. (a-b) Identification results for cell 1 (regularly shaped) and cell 2 (irregularly shaped); (c-d) Distance distributions between mitochondria and the cell nucleus or cell membrane in cell 1 and 2;(e-f) Distributions of the absolute and relative distances between mitochondria and the cell nucleus for cell 1 and 2;(g) Distribution of the mean relative distances (blue) and absolute distances (orange) between mitochondria and the cell nucleus. Each dot in (e-f) represents individual mitochondria while dots in (g) represent cell-level data. Scale bars in (a-b) represent 10 μm.

We found that in both "regular" and "irregular" cells (as shown in Fig. 4(a-b)), the distribution of distances between mitochondria and the nucleus or membrane exhibited consistent trends (Fig. 4(c-d)). After careful examination of the cell images shown in (a) and (b), one found that mitochondria tends to cluster in the directions of the cell growth. This is consistent with literature reports (for example, [22]). As the cells have radically different sizes and shapes, we define the

Biomedical Optics EXPRESS

relative distances, $D^{rel}_{mito-nuc}$ and $D^{rel}_{mito-mem}$, which are ratios of the mitochondria to the nucleus or the cell membrane with respect to the distance between the nucleus and membrane (i.e. a measure of the cell width) versus angle. For details of the calculation, please refer to the Materials and Methods section. The results are shown in Fig. 4(e-f), where we observed that even though the distributions are wide for both the relative and absolute distance of mitochondria, the mean of the relative distances were around 0.4-0.5 in both regular and irregular cells. For the absolute distances between mitochondria and the nucleus, however, they were significantly different in regular and irregular cells. Considering that the cell types and culture conditions were the same, these differences in absolute distances were likely due to variations in cell size and shape. Therefore, we believe that when analyzing the spatial distribution of mitochondria within cells, relative distances may be more meaningful than absolute distances. To further support this, we analyzed mitochondria in 10 cells with results shown in Fig. 4(g). Note here each dot represents cell-level data. For the mitochondria distribution within other 8 cells, please refer to Supplement 1 Fig. S4 for details. The mean values of the absolute and relative distances are used to plot Fig. 4 g. One can see that despite the wide range of absolute distances of mitochondria from the nucleus (10-20μm, with a coefficient of variation of ~23%), the mean relative distribution was confined to the range of 0.4-0.6 with a coefficient of variation of ~12%, further confirming the consistency of mitochondrial distribution within a given cell line.

3.4. Distribution changes of DRP1 and mitochondria in apoptotic cells

Studies have shown that mitochondrial fission events increase during apoptosis [31], with DRP1 accumulating more prevalently on mitochondria [26,32]. Usually such studies rely on labeling both DRP1 and mitochondria, and only few isolated regions of interest are selected for analysis. Here we use OS-PCM to label only DRP1 without labeling mitochondria, and obtain the spatial information of both structures and their changes within the whole cell during apoptosis. Here, the apoptosis is induced through treating cells with Ionomycin (More details in Supplement 1).

Figure 5 shows the changes in mitochondria and DRP1 aggregates induced by apoptosis compared to the control group. As shown in Fig. 5(a) and (b), the apoptotic cells exhibit evident membrane shrinkage, and the mitochondria also move closer to the cell nucleus compared to the normal cell. To quantify the changes due to apoptosis, we selected nine cells from each group and analyzed the distributions of DRP1 and mitochondria. Since there are many mitochondria and DRP1 aggregates in a cell, the mean values of the relative distance computed from each cell are used to represent the cell-level data. Firstly, we examined whether apoptosis altered their relative positions. From the results shown in Fig. 5(c) and (d), one can see that the relative position of mitochondria does not show significant changes while DRP1 distribution moves closer to the nucleus. Taking into account the increase in DRP1 aggregates during apoptosis, this may imply that during apoptosis DRP1 aggregates undergo growth near the cell nucleus or that DRP1 aggregates in the periphery of the cell converge towards the nucleus at a faster rate than the contraction of the cell membrane. We will further explore this issue in the following section. Figure 5(e) demonstrates that during apoptosis, the number of DRP1 aggregates located on mitochondria increases, indicating that DRP1, as expected, may be involved in mitochondrial fission during cell apoptosis [26]. Another example of the cell images showing DRP1 and mitochondrial changes during apoptosis can be found in Supplement 1 Fig. S5.

In order to further investigate changes in DRP1 during apoptosis, we conducted time-lapse observation and analysis of cells after adding 4μM ionomycin, with results shown in Fig. 6. Figure 6(a) shows the merged snapshots of DRP1 with mitochondria and the cell landmarks at 0, 15 minutes, and 30 minutes. One can see that mitochondria shrink, while DRP1 aggregates increase significantly during apoptosis. Next, we analyzed the complete time course, where Fig. 6(b) shows an increase in both the total number of DRP1 aggregates and the number of DRP1 aggregates on mitochondria. However, the proportion of DRP1 aggregates on mitochondria

Biomedical Optics EXPRESS

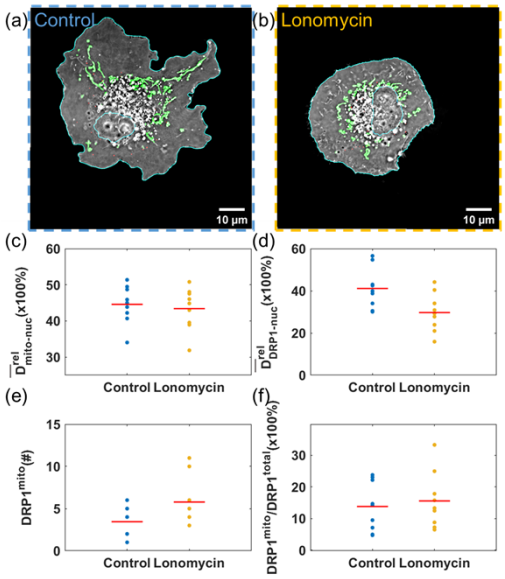

Fig. 5. Changes of DRP1 and mitochondria during apoptosis. (a-b) exemplary cell images from the control and the treatment group (green: mitochondria; red: DRP1 aggregate; blue: nucleus; cyan: cell membrane). (c-d) Distribution of the mean relative distance for mitochondria and DRP1 from the cell nucleus respectively; (e) Number of DRP1 aggregates co-localized with mitochondria. (f) Among the total DRP1 aggregates, the ratio of aggregates that are co-localized with mitochondria. Each dot in (c-f) represents a cell-level data. Scale bars in (a-b) represent 10 μm

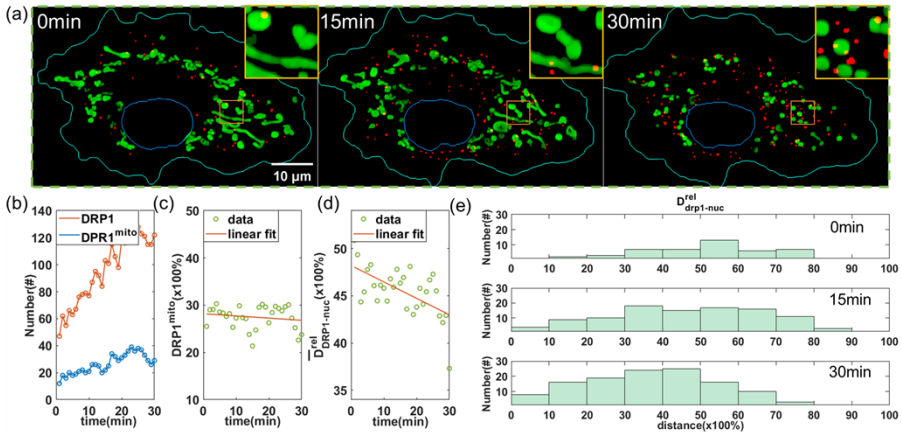

Fig. 6. Time course of DRP1 during apoptosis. (a) Cellular images at three time points: 0, 15 and 30 minutes (where the color representation is the same as Fig. 4(a)); (b) Total number of DRP1 aggregates (orange) and the number of DRP1 aggregates on mitochondria (blue); (c) Proportion of DRP1 aggregates on mitochondria among the total DRP1 aggregates; (d) The mean relative distance between DRP1 aggregates and the cell nucleus; (e) Distribution of the absolute distances between DRP1 and the cell nucleus at 0, 15 and 30 minutes after adding ionomycin. Scale bar in (a) represents 10 μm.

Biomedical Optics EXPRESS

with respect to the total number of the aggregates does not show significant change (Fig. 6(c)), consistent with the results shown in Fig. 5(f). Here only ~27% of DRP1 aggregates co-localize with mitochondria. By analyzing the spatial relationship between DRP1 and the nucleus (as shown in Fig. 6(d)), we found that during apoptosis, DRP1 aggregates tend to appear more frequently in the vicinity of the cell nucleus. In order to analyze the generation site of new DRP1 aggregates during apoptosis, we calculated the relative distance between DRP1 and the nucleus at 0, 15 and 30 minutes after treatment with results shown in Fig. 6(e). One finds that compared to 0 minutes, the number of DRP1 aggregates increases everywhere at 15 minutes; At 30 minutes, the number of aggregates within 50% of the relative distance from the nucleus increased, while the number of aggregates exceeding 50% decreased. From this we may conclude that the main reason for the decrease in average distance $D_{DRP1-nuc}$ is due to the newly formed DRP1 aggregates near the nucleus and the movement of DRP1 toward the nucleus.

4. Summary and discussion

In this paper, we have taken our previously reported OS-PCM paradigm, and extended it to make full use of the fluorescence channel within the system to allow for the correlation study of the spatial distribution and interactions between organelles and proteins with minimal labeling. This technique utilizes high-resolution phase contrast microscopy and a CNN network to obtain label-free information about organelles and other cellular landmarks. Simultaneously, the coupled fluorescence channel provides location information for proteins of interest, which, due to their small sizes and lack of refractive index contrast are still beyond the reach of phase microscopy systems. By automatic fusion and analysis of these two channels, along with their temporal changes, one can easily investigate protein-organelle interactions while simultaneously minimizing experimental complexity as well as potential label-induced interference to the cell. In this study, we demonstrate the proof-of-concept by examining the distribution and interactions of mitochondria and DRP1 under different physiological conditions. We found for the first time that, in COS7 cells, the mitochondria tends to regulate its position medially between the nucleus and cell membrane, regardless of the shape and size of the cells. Compared to the absolute distance from the nucleus (which is currently used in analyzing the spatial distribution of organelles and proteins) [7], the relative distance is a better metric because it can overcome the heterogeneity in shapes and sizes of the cell. During apoptosis, the ratio of DRP1 aggregates on mitochondria with respect to the total DRP1 aggregates does not increase significantly despite the fact that more DRP1 aggregates are indeed co-localized with mitochondria. At the same time, by utilizing the high resolution and high contrast original phase image, we can quickly determine that those DRP1 aggregates not on mitochondria were primarily localized to the ER. Note that here we have limited the study to relatively thin cells (such as COS7) where the mitochondria, membrane, and nucleus can be reasonably co-planar as the analysis is based on 2D images. With axial scanning, it is possible to use our system for 3D correlation study provided that the associated neural networks are trained on 3D data as well. Further, the OS-PCM concept should be transferrable to other high-resolution quantitative phase microscopy techniques such as holo-tomographic microscopy and optical diffraction tomography [15,33] using accordingly-trained neural networks.

In our results, we demonstrate several quantitative metrics such as the number of DRP1 aggregates and the co-localization count with mitochondria which are typically reported through multiple labeling, with our results (obtained with a single label) matching those of prior literature reports [26]. However, mitochondria, as sensitive cellular organelles and stress responders, are highly susceptible to the influence of high-intensity laser excitation, commonly used in fluorescence imaging, as well as concomitant oxidative stress. Traditional methods utilizing fluorescence labeling to observe their dynamic behavior may not accurately represent their true behavior and functionality. OS-PCM, by contrast, allowed us to reduce the quadruplex labeling to a single stain, simplifying the sample preparation significantly. Importantly, it completely

Biomedical Optics EXPRESS

removes the need to label large, high-volume landmark structures, substantially reducing the potential for photo-toxicity. This provides a more accurate representation of the true behavior and functionality of mitochondria and allows for a better understanding of their interactions with DRP1 and other cellular components. Further due to the availability of the whole-cell data, we can compute cell-level parameters (such as the mean distances and the ratio of DRP1 on mitochondria).

The keys to the above success are (1) the high spatial and temporal resolution of our ultra-oblique illumination phase contrast microscope, which enables individual organelles to be resolved and tracked continuously; (2) digital labeling of the organelles from the unlabeled cell images based on deep learning, which allows facile, automatic analysis of protein-organelle localization, as well as fission, fusion, and other dynamic organelle information; and (3) combining this with traditional fluorescence imaging, which "handles" imaging molecular targets that cannot be imaged by traditional phase contrast. Thus, our method is synergistic with previously developed fluorescence-based protocols and techniques. Further, OS-PCM, as it starts from a panoramic phase image, preserves the ability for the experimenter to return to the original phase image and trace down unexpected behaviors. For example, in this study we showed that non-mitochondrial DRP1 were primarily localized on the ER, which was also the source of new DRP1 aggregates during apoptosis. In a traditional fluorescence imaging experiment, if the ER was not labeled by the experimenter beforehand, they would be "blind" to its position. In OS-PCM, by contrast, the locations of all of the membrane bound organelles are simultaneously available. Therefore, our method holds great promise for future label-free visualization and automatic analysis of pan-organelle dynamics, including their mutual interactions, with minimum perturbation to the cell.

Funding. Anhui Provincial Key Research and Development Plan ((202003a07020020); National Key Research and Development Program of China (2017YFA0505300).

Disclosures. The authors declare no conflicts of interest.

Data availability. Source data are available from the corresponding author upon reasonable request. The customized MATLAB codes can be found at [34].

Supplemental document. See Supplement 1 for supporting content.

References

1. A. Jain and R. Zoncu, "Organelle transporters and inter-organelle communication as drivers of metabolic regulation and cellular homeostasis," Mol. Metab. **60**, 101481 (2022).
2. W. A. Prinz, A. Toulmay, and T. Balla, "The functional universe of membrane contact sites," Nat. Rev. Mol. Cell Biol. **21**(1), 7–24 (2020).
3. S. Park, J. S. Yang, Y. E. Shin, *et al.*, "Protein localization as a principal feature of the etiology and comorbidity of genetic diseases," Mol. Syst. Biol. **7**(1), 494 (2011).
4. W. K. Ji, R. Chakrabarti, X. Fan, *et al.*, "Receptor-mediated Drp1 oligomerization on endoplasmic reticulum," J Cell Biol **216**(12), 4123–4139 (2017).
5. W. K. Ji, A. L. Hatch, R. A. Merrill, *et al.*, "Actin filaments target the oligomeric maturation of the dynamin GTPase Drp1 to mitochondrial fission sites," eLife **4**, e11553 (2015).
6. P. P. Laissue, R. A. Alghamdi, P. Tomancak, *et al.*, "Assessing phototoxicity in live fluorescence imaging," Nat. Methods **14**(7), 657–661 (2017).
7. Q. Ba, G. Raghavan, K. Kiselyov, *et al.*, "Whole-Cell Scale Dynamic Organization of Lysosomes Revealed by Spatial Statistical Analysis," Cell Rep. **23**(12), 3591–3606 (2018).
8. A. M. Valm, S. Cohen, W. R. Legant, *et al.*, "Applying systems-level spectral imaging and analysis to reveal the organelle interactome," Nature **546**(7656), 162–167 (2017).
9. Y. Park, C. Depeursinge, and G. Popescu, "Quantitative phase imaging in biomedicine," Nat. Photonics **12**(10), 578–589 (2018).
10. Z. Wang, L. Millet, M. Mir, *et al.*, "Spatial light interference microscopy (SLIM)," Opt. Express **19**(2), 1016–1026 (2011).
11. E. Moen, D. Bannon, T. Kudo, *et al.*, "Deep learning for cellular image analysis," Nat. Methods **16**(12), 1233–1246 (2019).
12. T. Wen, B. Tong, Y. Liu, *et al.*, "Review of research on the instance segmentation of cell images," Comput Methods Programs Biomed **227**, 107211 (2022).

Biomedical Optics EXPRESS

13. E. M. Christiansen, S. J. Yang, D. M. Ando, *et al.*, "In Silico Labeling: Predicting Fluorescent Labels in Unlabeled Images," Cell **173**(3), 792–803.e19 (2018).
14. C. Ounkomol, S. Seshamani, M. M. Maleckar, *et al.*, "Label-free prediction of three-dimensional fluorescence images from transmitted-light microscopy," Nat. Methods **15**(11), 917–920 (2018).
15. Y. Jo, H. Cho, W. S. Park, *et al.*, "Label-free multiplexed microtomography of endogenous subcellular dynamics using generalizable deep learning," Nat. Cell Biol. **23**(12), 1329–1337 (2021).
16. S. Guo, Y. Ma, Y. Pan, *et al.*, "Organelle-specific phase contrast microscopy enables gentle monitoring and analysis of mitochondrial network dynamics," Biomed. Opt. Express **12**(7), 4363–4379 (2021).
17. J. Lee, H. Kim, H. Cho, *et al.*, "Deep-Learning-Based Label-Free Segmentation of Cell Nuclei in Time-Lapse Refractive Index Tomograms," IEEE Access **7**, 83449–83460 (2019).
18. A. Somani, A. Ahmed Sekh, I. S. Opstad, *et al.*, "Virtual labeling of mitochondria in living cells using correlative imaging and physics-guided deep learning," Biomed. Opt. Express **13**(10), 5495–5516 (2022).
19. Y. Ma, S. Guo, Y. Pan, *et al.*, "Quantitative phase microscopy with enhanced contrast and improved resolution through ultra-oblique illumination (UO-QPM)," J Biophotonics **12**(10), e201900011 (2019).
20. J. Fang, H. Zhang, Y. Pan, *et al.*, "Label-Free Analysis of Organelle Interactions Using Organelle-Specific Phase Contrast Microscopy (OS-PCM)," ACS Photonics **10**, 1093–1103 (2023).
21. H. Zhang, J. Fang, Y. Dai, *et al.*, "Rapid Intracellular Detection and Analysis of Lipid Droplets' Morpho-Chemical Composition by Phase-Guided Raman Sampling," Anal. Chem. **95**(36), 13555–13565 (2023).
22. M. P. Viana, J. Chen, T. A. Knijnenburg, *et al.*, "Integrated intracellular organization and its variations in human iPS cells," Nature **613**(7943), 345–354 (2023).
23. V. Eisner, M. Picard, and G. Hajnoczky, "Mitochondrial dynamics in adaptive and maladaptive cellular stress responses," Nat. Cell Biol. **20**(7), 755–765 (2018).
24. W. Chen, H. Zhao, and Y. Li, "Mitochondrial dynamics in health and disease: mechanisms and potential targets," Signal Transduction Targeted Ther. **8**(1), 333 (2023).
25. T. B. Fonseca, A. Sanchez-Guerrero, I. Milosevic, *et al.*, "Mitochondrial fission requires DRP1 but not dynamins," Nature **570**(7761), E34–E42 (2019).
26. S. Frank, B. Gaume, E. S. Bergmann-Leitner, *et al.*, "The role of dynamin-related protein 1, a mediator of mitochondrial fission, in apoptosis," Dev. Cell **1**(4), 515–525 (2001).
27. D. Mahecic, L. Carlini, T. Kleele, *et al.*, "Mitochondrial membrane tension governs fission," Cell Rep. **35**(2), 108947 (2021).
28. J. A. Mears, L. L. Lackner, S. Fang, *et al.*, "Conformational changes in Dnm1 support a contractile mechanism for mitochondrial fission," Nat. Struct. Mol. Biol. **18**(1), 20–26 (2011).
29. A. Lefebvre, D. Ma, K. Kessenbrock, *et al.*, "Automated segmentation and tracking of mitochondria in live-cell time-lapse images," Nat. Methods **18**(9), 1091–1102 (2021).
30. T. Kleele, T. Rey, J. Winter, *et al.*, "Distinct fission signatures predict mitochondrial degradation or biogenesis," Nature **593**(7859), 435–439 (2021).
31. R. J. Youle and M. Karbowski, "Mitochondrial fission in apoptosis," Nat. Rev. Mol. Cell Biol. **6**(8), 657–663 (2005).
32. A. Jenner, A. Pena-Blanco, R. Salvador-Gallego, *et al.*, "DRP1 interacts directly with BAX to induce its activation and apoptosis," EMBO J. **41**(8), e108587 (2022).
33. P. A. Sandoz, C. Tremblay, F. G. van der Goot, *et al.*, "Image-based analysis of living mammalian cells using label-free 3D refractive index maps reveals new organelle dynamics and dry mass flux," PLoS Biol. **17**(12), e3000553 (2019).
34. C. Chen, Z. Smith, J. Fang, *et al.*, "Distance Analysis," figshare, 2019, https://doi.org/10.6084/m9.figshare.24416677.v3